

# Stability analysis of low-n modes for the Divertor Tokamak Test facility

## Single Null Scenario

V. Fusco, G. Vlad, G. Fogaccia, E. Giovannozzi

*ENEA, FSN, C. R. Frascati, Via E. Fermi 45, 00044 Frascati (Roma), Italy*

### Introduction

The Divertor Tokamak Test (DTT) [1] is a new facility that will be hosted in Frascati, Italy. The main purpose of the DTT tokamak is to investigate and design a specific component, the so-called divertor, whose aim is to exhaust energy associated to charged particles that escape the confining magnetic field. In this work the so-called SN (single null) Full power (45MW within the following ranges of different heating system: 26-36 MW of ECRH, 3-9 MW of ICRH and 7.5-15MW of NNBI) scenario proposed for DTT is studied [2]. The scenario is characterized by a flat top plasma current  $I_p=5.5$  MA, a vacuum toroidal magnetic field  $B_0=5.85$  T, a major plasma radius  $R_0=2.19$ . At the most fundamental level, it is imperative to find a macroscopic equilibrium state for the plasma and to study its magnetohydrodynamic (MHD) stability as a prerequisite to allow operation of plasma fusion devices and prevent bad plasma performances and/or plasma wall damages. In this study, our attention is focused on low toroidal (n) stability for both ideal and resistive plasmas, keeping high n mode studies to a future work.

### MHD Analysis

The simulation analysis carried out in this work uses the profiles obtained by the electromagnetic analyses (CREATE-NL [3]) and the transport analyses (JETTO [4]); in particular, for this study, we consider a steady state plasma scenario as result of transport simulations. The transport solver supplies the plasma current and pressure profiles but stability analyses require higher resolution than the one provided by transport solvers. Thus, to this aim, we use the equilibrium solver CHEASE [5], a high-resolution fixed boundary code that solves the Grad-Shafranov equation in toroidal geometry, assuming static MHD equilibria and axisymmetry. MARS [6] is the stability code used. It solves full MHD linear, resistive equations, it considers a two dimensional, axisymmetric general toroidal geometry carried out in flux coordinate  $(s, \chi, \phi)$  where  $s=(1-\psi/\psi_{axis})^{1/2}$  is the poloidal radial-like coordinate, such that  $s=0$  on axis and  $s=1$  on the plasma edge,  $\psi$  is the poloidal flux function,  $\chi$  is a generalized poloidal angle and  $\phi$  is the geometrical toroidal angle. MARS can also

consider a vacuum region between the plasma last closed surface and a perfectly conducting wall, assumed to be conformal to the plasma last closed magnetic surface.

In the framework of DTT MHD analysis, the relevant parameters are the safety factor and

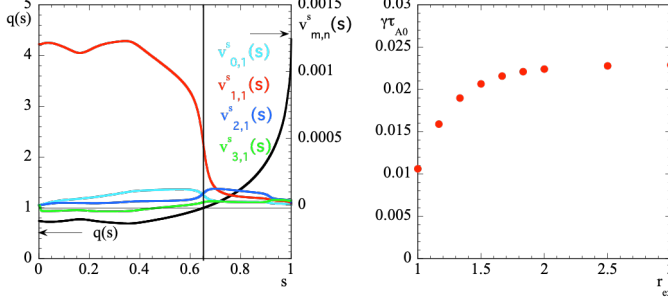


Fig.1 L.h.s: Contravariant components of the perturbed velocity  $v^s_{m,n}(s)$  for the internal kink mode  $(m,n)=(1,1)$  vs  $s$  at  $r_{\text{ext}}=3$  and the safety factor  $q$  vs  $s$ . R.h.s: Internal kink growth rate normalized to the inverse of the on axis Alfvén time  $\tau_{A0}$  ( $\tau_{A0}=R_0\sqrt{(\mu_0\rho_0)/B_0}$ ),  $\rho_0$  is the on axis mass density) vs the perfectly conducting wall position  $r_{\text{ext}}$ .

magnetic field,  $\langle p \rangle$  the pressure averaged on the plasma volume; the pressure peaking  $p_0/\langle p \rangle$ , with  $p_0$  the pressure on axis, is approximately equal to 4. Because of the  $q=1$  surface inside the plasma, an internal kink is expected. Indeed, an unstable internal kink  $(m,n)=(1,1)$  is found by the MARS code located within the  $q=1$  rational surface (left hand side (l.h.s.) of

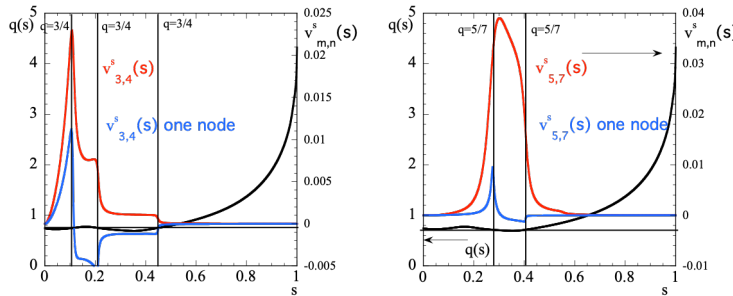


Fig.2 L,h,s: Contravariant component of the perturbed velocities  $v^s_{m,n}(s)$  vs  $s$  for the  $(m,n)=(3,4)$  and  $(m,n)=(5,7)$  infernal modes: main perturbation (red) and single radial node perturbation (blue).

normalized growth rate  $\gamma$ , as a function of the wall position  $r_{\text{ext}}$ : it demonstrates we are dealing with an internal mode, although the dependence of the growth rate from the wall position implies the presence of an external mode component as well. It's worth noting that such large  $q=1$  position should be avoided because the internal kink could be responsible of sawtooth crash; in this case only a slightly beneficial effect on the control of  $q=1$  location is provided by ICRH and ECRH available [7]. On the other hand, the addition of sawtooth model in a transport code is a work in progress which could result in a  $q=1$  smaller radius thus allowing a better control by external heating sources [8].

the  $\beta$  profiles. The safety factor  $q$  is quite flat around the plasma center, it's value on axis is  $q_0=0.7$  and at the edge is  $q_{95\%}=2.8$ ; the  $q=1$  is located around  $s \approx 0.64$ . The toroidal beta is  $\beta_{\text{tor}}=1.89\%$ ,

defined as  $2\mu_0\langle p \rangle/B_0$ , where  $\mu_0$  is the vacuum permeability constant,  $B_0$  the on axis

Fig.1). The conducting wall is supposed to be placed far away from the plasma wall at  $r_{\text{ext}}=3$ ;  $r_{\text{ext}}$  is defined as the ratio  $b/a$ , where  $a$  is the plasma minor radius and  $b$  is the wall minor radius.

Fig.1, right hand side (r.h.s), shows the

When increasing the toroidal mode number  $n$ , the so-called infernal modes are found;

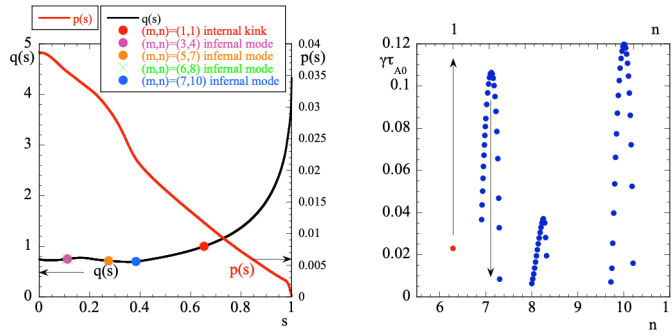


Fig.3 L,h,s: Position of the internal kink and infernal modes on the safety factor  $q(s)$  and pressure profile  $p(s)$ . R.h.s: Oscillatory behavior of the infernal modes growth rate, the red dot is the internal kink of the growth rate.

these modes can limit the achievable performance of the machine [9]. The infernal mode is a pressure driven internal MHD instability, characterized by low to intermediate toroidal  $n$

and poloidal  $m$  mode numbers, which is excited in a region of low shear and high pressure gradient. Examples of radial perturbed velocities  $v_{m,n}^s(s)$  for infernal modes as obtained by MARS for this scenario are presented in Fig.2; it's worth noting the single radial node modes (see Fig. 2) have always smaller growth rate than the main modes.

The position of the infernal modes w.r.t the safety factor profile is represented in Fig.3. Moreover, the oscillatory behavior of the infernal modes growth rate, with respect to  $n$  (here considered as a continuous parameter), is depicted in Fig.3 r.h.s [10]. For comparison, the growth rate of the internal kink is also reported with a red dot and it is clear that the infernal modes oscillatory behaviour makes it difficult to predict which  $n$  value will give the most unstable mode.

### Sensitivity Analysis

Sensitivity analysis on relevant quantities such as the safety factor on axis  $q_0$  and  $\beta$  has been carried on as well. In Table 1 (l.h.s.),  $q_0$  is changed keeping constant the other relevant quantities; vice versa, in the r.h.s,  $\beta_{\text{tor}}$  is changed and the other quantities are kept constant. Here the  $\beta_N$ , normalized, is defined as  $\beta_N = \beta_{\text{tor}} / I_p / (aB_0)$ .

q	$I_{\text{tot}}$ MA	$q_0$	$q_{95\%}$	$q_{\text{edge}}$	$\beta_{\text{tor}}\%$	$\beta_N\%$	p	$I_{\text{tot}}$ MA	$q_0$	$q_{95\%}$	$q_{\text{edge}}$	$\beta_{\text{tor}}\%$	$\beta_N\%$
—	5.489	0.74	2.8450	4.3	1.89	1.20	p0	5.489	0.74	2.8450	4.3	1.89	1.20
—	5.487	0.82	2.8747	4.0016	1.866	1.191	0.5p0	5.505	0.75	2.82	4.2	0.0096	0.73
—	5.327	1.10	2.9072	3.999	1.803	1.328	1.5p0	5.475	0.71	2.87	4.4	2.81	1.81
—	5.315	1.3	2.9636	4.0067	1.675	1.263	2p0	5.459	0.69	2.90	4.5	3.72	2.43
—	5.131	1.5	2.9965	4.0087	1.606	1.086	2.5p0	5.444	0.67	2.93	4.6	4.64	3.04

Table 1. L.h.s: The safety factor on axis  $q_0$  is varied. (R.h.s): The  $\beta$  ( $\beta_{\text{tor}}$  or  $\beta_N$ ) is varied.

The results of stability runs for the cases equilibria shown in Table1 (l.h.s) are summarized in Fig.4 (l.h.s.) where the position of infernal modes, internal kink and external modes on  $q$  rational surfaces are reported: the internal kink  $(m,n)=(1,1)$  does exist as long as  $q_0 \leq 1$ , the infernal modes are revealed when  $q$  rational surfaces are intercepted in the zone of low shear

and high pressure gradient, the  $(m,n)=(2,1)$  external modes appear when the  $q$  is quite far from the nominal scenario; Fig.4 (r.h.s) shows their normalized growth rate.

The plot in Fig.5 (l.h.s), depicts the radial perturbed velocity  $v_{2,1}^s(s)$  of the external mode and the  $q$  profile (orange  $q$  case of Table 1 (l.h.s)) whilst Fig.5 (r.h.s) shows its growth rate

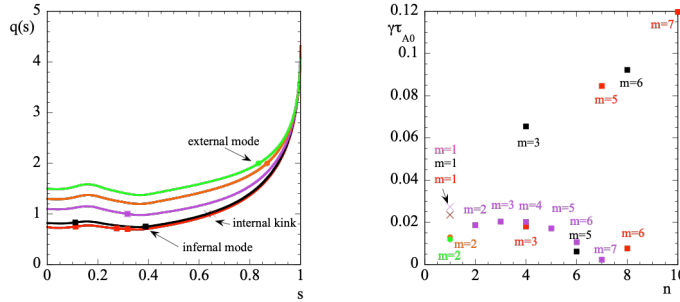


Fig.4 L.h.s. Positions of the infernal modes (squares), internal kink (crosses) and external modes (full circles) on the different safety factor  $q$  from Table 1. R.h.s: normalized growth rate vs  $n$  for the modes. Each color corresponds to the  $q$  considered and the symbols to the different modes; poloidal modes number are shown as well.

Table 1 (r.h.s.), the  $q$  profile slightly changes, whilst the pressure is varied. Internal kink and

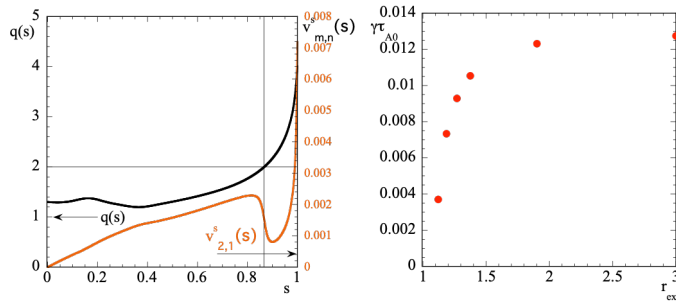


Fig.5 L.h.s: Contravariant component of the perturbed velocities  $v_{m,n}^s(s)$  vs  $s$  for the  $(m,n)=(2,1)$  external mode and  $q$  profile vs  $s$  in arbitrary units. R.h.s: Growth rate normalized to the Alfvén time of the external mode vs the perfectly conducting wall position  $r_{ext}$ .

versus the ideally conducting wall position  $r_{ext}$ . Such mode disappears when the wall is placed on the plasma surface ( $r_{ext}=1$ ) demonstrating the external nature of the mode. As concern the stability analysis for the equilibria reported in

internal modes are still revealed because the  $q$  profile is almost untouched but, when the  $\beta$  is high enough, an external mode  $m,n=2,2$  appears as well.

Anyway, as for the previous sensitivity analysis w.r.t.  $q_0$ , it is

important to emphasize that this situation is very far ( $2.5 \times p_0$ ) from the nominal case. Finally, when resistivity is added in the analysis, the qualitative and quantitative behaviour of the mode exhibits little changes, and no specific resistive modes are observed.

[1] R. Martone, R. Albanese, F. Crisanti, A. Pizzuto, P. Martin. "DTT Divertor Tokamak Test facility Interim Design Report, ENEA (ISBN 978-88-8286-378-4), April 2019 ("Green Book")" <https://www.dtt-dms.enea.it/share/s/avvglhVQT2aSkSgV9vuEtw>. [2] Casiraghi et al, Nucl.Fusion 61, 2021, 116068. [3] R. Albanese et al., Fusion Engineering and Design 96–97 (2015) 664–667. [4] Cenacchi G. and Taroni A. 1988 ENEA-RT-TIB 88-5 ENEA. [5] H. Lütjens, et al., 97, Issue 3, 1996, Pages 219-260. [6] A. Bondeson, G. Vlad, and H. Lütjens. Physics of Fluids, B4:1889–1900, 1992 [7] S. Nowak, private communication [8] F. Porcelli et al 1996 Plasma Phys. Control. Fusion 38 2163 [9] A. Fasoli, Computational challenges in magnetic-confinement fusion physics, NATURE PHYSICS | VOL 12 | MAY 2016 [10] J. Manickam et al 1987 Nucl. Fusion 27 1461